



# Resilient by design: Preventing wildfires and blackouts with microgrids

Weijia Yang<sup>\*</sup>, Sarah N. Sparrow, Masaō Ashtine, David C.H. Wallom, Thomas Morstyn

Department of Engineering Science, University of Oxford, Parks Road, OX1 3PJ, United Kingdom  
School of Engineering, University of Edinburgh, EH8 9YL, United Kingdom

## HIGHLIGHTS

- A novel strategy for managing wildfires and blackouts using microgrids is proposed.
- The Fire Weather Index is used to describe the fire risk distribution in a grid.
- The Grid and Wildfire Index are linked by line locations and fire risk distribution.
- Set Victoria Australia as a case study, 68% of the overall system cost can be saved.

## ARTICLE INFO

### Keywords:

Distributed generation  
Fire weather index  
Geospatial model  
Grid resilience  
Networked microgrid

## ABSTRACT

This paper proposes a strategy for managing wildfire risks and preventing blackouts using microgrids. To demonstrate this approach, not seen in previous literature, we use the power network of Victoria, Australia, in December 2019 as a case study. The Fire Weather Index (FWI) is a crucial indicator of global fire behaviour both spatially and temporally, as proved with its robust analysis within many previous studies. The FWI is applied to a Wildfire-Energy System for the first time, contributing to a higher spatial and temporal resolution to position the wildfire risk in a grid. A novel method is proposed to automatically correlate the wildfire risk index and the power network model using geographical information of the transmission lines. The optimal power flow and grid performances are obtained from a grid model which incorporates wildfire risk distributions. It is shown that a system with installed microgrids can maintain operation under severe fire-related conditions without scheduled or unplanned outages. Finally, a cost-benefit analysis is conducted, which demonstrates that 68% of system costs can be recuperated by implementing networked microgrid solutions.

## 1. Introduction

In recent years, the frequency of extreme weather events has increased worldwide, in part due to climate change, resulting in significant financial and social losses to both power system operators and consumers [1]. Wildfires are initiated by different causes, either natural (such as lightning strikes) or human (e.g., accidental sparks, or deliberate arsons). The predominant cause of wildfires is different in various regions, e.g., human factors account for about 42.9% of ignitions in Victoria, Australia [2], whereas 95% of ignitions attribute to human activities in California [3]. Fuel flammability, low humidity, and high wind conditions can all increase the probability of extreme wildfire conditions [4]. With increasingly frequent wildfires, heat damage to grid infrastructure can occur and lead to the introduction of further hazards [5]. Specific hazards to the energy infrastructure include sagging

conductor lines due to the high temperatures during the wildfire season and flashover events [6].

Wildfire risks to the grid have become an international phenomenon in recent years. For instance, from December 2019 to February 2020, Australia faced an unprecedentedly intense and devastating wildfire season [7]. Multiple wildfires broke out in all states in Australia, particularly in Victoria, resulting in 34 fatalities and the destruction of more than 10 million hectares of land [8,9]. Approximately 20,000 households' power supplies were disconnected at the peak of wildfires during the New Year period in New South Wales [10]. Also, in 2018, a transmission line belonging to California's largest utility, Pacific Gas & Electric (PG&E), started a wildfire that led to the company pleading guilty to 84 counts of manslaughter and destruction of the Town of Paradise [11]. This devastating wildfire caused around \$13.5 billion of damage to property, such that PG&E was forced to declare bankruptcy

<sup>\*</sup> Corresponding author.

E-mail address: [weijia.yang@eng.ox.ac.uk](mailto:weijia.yang@eng.ox.ac.uk) (W. Yang).

<https://doi.org/10.1016/j.apenergy.2022.118793>

Received 15 October 2021; Received in revised form 28 January 2022; Accepted 18 February 2022

Available online 8 March 2022

0306-2619/© 2022 The Authors. Published by Elsevier Ltd. This is an open access article under the CC BY license (<http://creativecommons.org/licenses/by/4.0/>).

[11]. In regions prone to wildfires, managing these low-probability and high-risk events has required frequent short-term disconnections, which affect millions of customers and add indirect social loss on top of physical loss.

The conventional power system has a one-way structure, with power delivered from generation to transmission, distribution, and demand [12]. Along with this structure, long-distance, high-voltage power lines traversing heavily forested areas are particularly vulnerable to wildfires [4]. According to a recent article in the San Francisco Chronicle, physical methods like undergrounding and better insulation of the overhead lines have been outlined by several states to enhance the grid resilience (defined as the ability of a grid to sustain normal operation under extreme conditions) with a greater wildfire risk [13]. Resilience is one of the key grid indicators, which can be improved by network design and physical reinforcements. Network resilience is defined as the ability of a power grid to sustain normal operation when facing high-impact, low probability events like natural hazards [14]. A resilient system should be endowed with fault tolerance, quick response, restorability, and reliability when facing disruptive events [15]. Both the load shedding rate and the line loading rate can be utilised to measure system resilience [16]. In our paper, four grid resilience metrics are utilised to assess the system resilience performance in different scenarios. The definitions, units and selection reasons for the metrics will be discussed in detail in Section 2.5.

The cost of physical reinforcements is prohibitively expensive: it is estimated that it will take over \$100 billion for PG&E to underground all its high voltage lines across their entire network (2/3 of California). Besides the significant expense, there is concern about the environmental effects of undergrounding in bio-diverse regions [13].

With an increasing pursuit of more robust and clean grid operations, the regulation and enhancement of grid resilience using renewables have attracted more public attention [17]. One such method is the use of microgrids. A microgrid is a subset of the network that can operate independently from other parts of the network, made up of small-scale distributed generations, local demand, and energy storage systems. In microgrid strategies, various Distributed Generators (DGs) are installed in the vicinity of end-users, such as photovoltaic (PV) panels and small wind turbines [18]. The capacity of DGs can range from several kilowatts to 300 MW [19].

In our paper, various capacities of distributed generators are installed at each node of a transmission network to share the load burden during wildfire seasons. According to regional wildfire risks, parts of the network transmission lines are disconnected, and the corresponding local demands are supported by the distributed generators to avoid load shedding as much as possible. The remaining operating lines in “fire-free areas” keep the power channel between nodal demand and the grid generation unobstructed. In this case, the nodal demand is partially supplied by either the main grid or the local distributed generation depending on the economic benefits (e.g., the real-time electricity price). The two operation modes above can represent the grid connection (i.e., normal mode) and the isolated islanding mode, thus being treated as a potential microgrid method to enhance the grid operation under extreme events.

Jazebi et al., 2020 provided a comprehensive review of previous wildfire management techniques in engineering-related fields. It was found that existing literature mainly focused on how wildfires may physically damage lines in high wildfire risk areas [20,21]. However, wildfire risks can affect grid performance without direct damage, e.g., soot accumulation may lead to current leakage and line off [5]. Solar photovoltaic power is not a recommended local DG source in fire-prone regions since the wildfire smoke negatively affects the power generation – the overall electricity reduction is 7%, with the peak power shedding of 27% in a fire-burn case study in Canberra [22]. Similar phenomena have been found in California and Malaysia – a 30% reduction in average electricity generation in California during September 2020 [23] and 0.43 W power reduction per increment of 1 point Air Pollution Index

(API) for Malaysian PV in 2014 [24]. More comprehensive influence factors should be considered in the future. Rhodes et al., 2020 created an optimisation model to mitigate powerline fire risk, based on the Institute of Electrical and Electronics Engineers-Reliability Test System of the Grid Modernization Laboratory Consortium test case in Southern California [4]. Power Shut-off methods were used to allow lines that were important for load delivery to continue to run even with high loading and high wildfire risks, whilst other lines with less load were disconnected at a lower wildfire risk. This control system enabled more load portions to be served in a high wildfire risk period. However, once the overloaded lines exceeded the tolerable time for the protection relay without microgrid supports, it would lead to load shedding and line outages [25]. This method may cause a powerline fire if the highly loaded lines operate for an extended period [6]. Thus, a strategy considering microgrids is motivated to sustainably serve more load without powerline fires and system failure for longer durations.

This paper proposes the novel use of microgrids to manage wildfire risks within power systems without resorting to power outages. As an extensively validated measure of fire potential, the Canadian Forest Service Fire Weather Index Rating System (FWI) is innovatively utilised to describe the wildfire risk distribution over a power grid. The previous study [4] utilised a static wildfire risk distribution model that was spatially partitioned into only three levels based on loosely assembled data from [26]. In comparison, in our study the wildfire risk is measured daily and regionally with exact ‘Danger Ratings’ to achieve a higher accuracy. In addition, a cost-benefit analysis of the proposed microgrid method is conducted to prove its feasibility and sustainability. The method in our paper is adaptable and can be applied to protect power networks in other fire-prone areas. The Wildfire-Energy System (hereafter the Test System) represents an example case of our model based on a practical grid scenario of Victoria, Australia, in the 2019–2020 wildfire season. The Test System consists of two main components: the Wildfire Index that calculates the wildfire risk distribution for Victoria, and the Grid Model that simulates the power network of Victoria, hereby refer to as the Wildfire Index and the Grid Model. Considering the economic and environmental limitations of the physical reinforcements, network improvements with microgrids are proposed in this paper to enhance the grid resilience during fire seasons.

In Section 2, the methodology to construct the Test System with geographical data is discussed in detail. The overview and dataset sources of the three scenarios are described in Section 3, aiming to explore how overall wildfire risks, FWI line disconnection thresholds and microgrids influence grid resilience. In Section 4, the results for the resilience performance analysis are demonstrated and analysed with four parameters, including line loading, load shedding, system operating costs, and carbon emission factors. The cost-benefit analysis for microgrid solutions is also discussed, and Section 5 summarises the main findings and advises potential future developments to the Test System.

## 2. Methodology

In this section, we describe the proposed method following the model formulation process. The Wildfire Index calculation and the Grid Model construction are first explained in Sections 2.1 and 2.2. A spatial analysis technique is then described to match the Grid Model with the Wildfire Index using the coordinates of transmission lines (as explained in Section 2.3). In this study, microgrid solutions are utilised to share regional demand when bulk supply is significantly reduced due to wildfires. Designs of microgrids and automatic line control strategies are also discussed in this section (as explained in Section 2.4).

Furthermore, the simulation methods used to assess system resilience are described as the critical analysis of this paper in Section 2.5. Direct Current Optimal Power Flow (DCOPF) has been implemented as the main simulation to calculate the optimal grid solution under system safety conditions, producing various performance indices. Fig. 1 shows the main components and the main steps to obtain grid resilience under

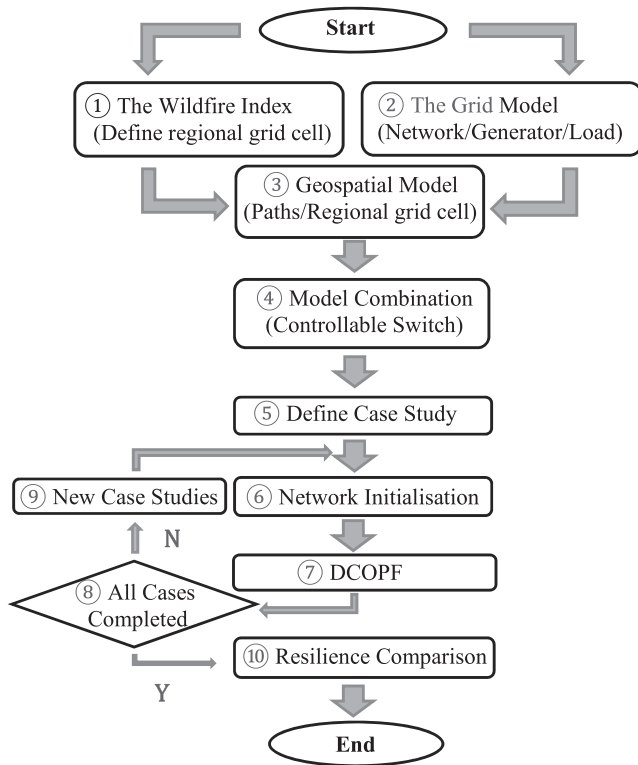


**Fig. 1.** Main components and construction steps flow chart for the Wildfire-Energy System.

fire risks in our model. This section describes general methods of power grid analysis under wildfire risks for increased replicability and model implementation across other regions of interest.

### 2.1. The wildfire index

The simulation of the wildfire risk distribution is one of the critical parts for the Test System design. Wildfire risk levels can have substantial simultaneous differences within a large country. Therefore, a better temporal and spatial accuracy of the wildfire risk severity is crucial to model the Test System better.

A weather-dependent risk index was utilised in our study to simulate the wildfire risk distribution during the 2019–2020 wildfire season. The FWI is a meteorological index that is used to evaluate the risk of wildfires [27]. The FWI ingests meteorological parameters such as temperature, wind speed, relative humidity and 24-hr precipitation [28]. The FWI *Danger Rating* (DR) is classified into six levels, and the relationship with FWI is described in Table 1.

An alternative index is the McArthur Forest Fire Danger Index (FFDI), developed based on Australia's wildfire data [29]. According to findings from Dowdy et al., 2009, both FWI and FDI were mostly sensitive to the wind, relative humidity, and temperature. The percentile of the two indices showed a consistent representation under severe fire

**Table 1**  
FWI Danger Rating classification adapted from [28]  
(upper bound excluded).

Fire Danger	FWI Ranges
Very Low	(0, 5.2)
Low	(5.2, 11.2)
Moderate	(11.2, 21.3)
High	(21.3, 38.0)
Very High	(38.0, 50.0)
Extreme	(50.0, +∞)

conditions [30]. In most cases, FFDI and FWI both offered similar climatological patterns of wildfires and resulted in similar warnings for wildfire disasters [31]. Thus, the wildfire distribution is relatively independent of the index used. Oldenborgh et al. have applied the FWI to analyse the attribution of Australian bushfires [32]. While FWI was originally derived from Canada, it has been shown to be applicable in many different climatic regions (e.g., Mediterranean Europe [33,34]). Therefore, FWI was utilised in this study based on the universality and the availability of the index.

The FWI of each microclimate region is available from the Copernicus Climate Data Store [29] in Network Common Data Format (netCDF) files [35]. A microclimate is defined as a region with specific climate conditions and topographic locations [36]. This paper describes a microclimate as a region with a different wildfire risk feature from neighbouring regions. For the case study area, the whole studied region was divided into  $0.25^\circ \times 0.25^\circ$  grid cells in line with the spatial resolution of the wildfire risk distribution data. As the geographical coverage of the data is on a global scale, the FWI distribution can be calculated for other regions using the same method [32]. As an example of wildfire risk distribution, Fig. 2 shows the Australian FWI for the 30<sup>th</sup> of December 2019, highlighting the wildfire risk danger level.

In previous studies, such as [32,33,34], FWI is used as a measure of fire risk irrespective of ignition sources. Determining the actual risk of powerline ignition at a particular FWI value is beyond the scope of this paper as we are unable to quantify the likely occurrence of all possible ignition sources at all locations. This is especially true given a number of ignition sources that are the direct result of human behaviour. In França et al., the FWI was utilised as one of the three main elements to assess the fire-risk-breakdown of the power lines in Northern Brazil [37]. Thus, the FWI was regarded as a reference index here to help determine the proper operating mode of the grid component within the Grid Model to avoid a larger scale outage. In practical power systems, the system operators should design a fire prevention plan considering both the regional FWI and possible ignition sources nearby.

### 2.2. The grid model

Three main steps to construct the Grid Model are explained in detail in this section. The power network was set up within the Grid Model in Step 1, the power generation information was added in Step 2, and the energy demand distribution was obtained in Step 3. The detailed construction procedures and data sources specific to the Victoria Case study are discussed in detail in Section 3.

It is notable that our model focuses on grid formation and static power dispatch rather than dynamic energy dispatch. Our grid resilience

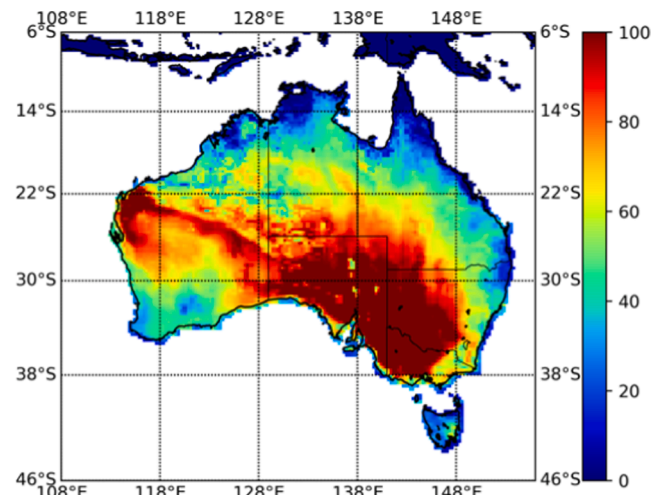


**Fig. 2.** Australia FWI colourmap on 30<sup>th</sup> Dec 2019.

analytical parameters are obtained for the worst-case scenario (when the grid is operating at peak load). The current work is assessed with dynamic wildfire risk simulations and grid at peak demand. We only consider wind generation with a capacity factor. However, future work could consider more detailed modelling of local microgrid load profiles, which would allow us to investigate the value of battery storage.

#### Step 1: Network Assembly

A Keyhole Markup Language (KML) file is a file format to display geographic data containing pinpoint locations and image overlays [38]. As input, raw KML data were downloaded to obtain the geographical and electrical information about transmission lines, substations, and power stations [39]. State and boundary data were imported in the format of shapefiles [40]. The Statistical Area Level 2 (SA2) population dataset [41] was obtained to estimate the regional demand distribution by the Voronoi tessellation method [42]. Then, the operational grid components belonging to National Electricity Market (NEM) zones were sorted based on the information from energy market operators [43]. As an example, the operational grid and the demand proportion served by each node within the state of Victoria are shown in Fig. 3.

#### Step 2: Generator Dataset

While the power station positions were given in Step 1, technical and economic parameters were assigned to generation information. The technical data of generators were collated, including fuel types and registered capacities. Databases containing the unit technical parameters and operating costs were imported to supplement the information in this step. After filtering generators that did not satisfy the system conditions (e.g., standing exemption of small-scale DGs according to the local authority), a comprehensive dataset that contained all the necessary generation information was obtained.

#### Step 3: Historical Load and Dispatch

Historical load signals were required to provide the actual demand

for the power flow simulation in *Pandapower* [39]. However, most of the public load dispatch data were regional rather than nodal demands divided into smaller clusters. The nodal demand distribution was obtained using the aforementioned method of Voronoi tessellation. Based on the output from Step 1, the nodal demand was attained by multiplying the total demand by the nodal proportion.

#### Networked Microgrids

In the microgrid scenario, networked microgrids were installed at each node of the Grid Model to enable the regional grid to transform between grid-connection and islanded mode flexibly. Different proportions of nodal demands were served with additional DG integrations to investigate how much load shedding of the Test System can be avoided with various capacities of microgrids. To be more specific, nodal demands were calculated from Step 3. Different nodal demand proportions were then supported with DGs to share the local demand, particularly at nodes isolated due to high fire risk. Finally, the whole system performance was assessed by comparing the result of resilience parameters (Table 2). A cost-benefit analysis was conducted to seek a better trade-off between the cost of load shedding and the microgrid installation solution.

#### 2.3. Geospatial modeling

The length and the trajectory of transmission lines are essential for the Test System, primarily because some electrical parameters (e.g., resistance) are closely related to the line length. Another reason is that knowing the exact path of lines (rather than only start points and end points) is essential for accurate wildfire risk detection of lines that cross multiple microclimates. To complement the Grid Model with network line geographical information, KML files containing multiple coordinates were utilised to describe the line paths with a higher accuracy.

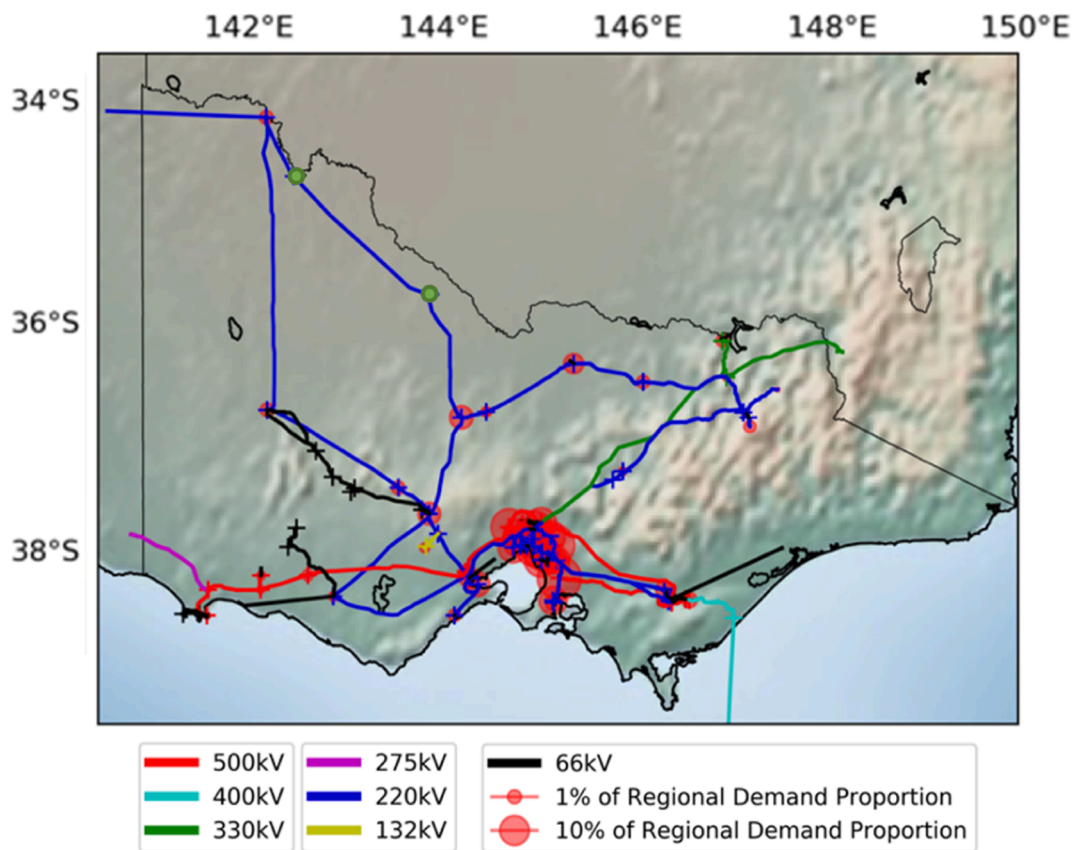


**Fig. 3.** High voltage transmission network in Victoria, Australia, where “+” represents substations, the size of red circles represents regional energy demand proportion, the two green spots indicate a 220 kV transmission line from Red Cliffs to Kerang, which will be discussed as an example in Section 2.4. (For interpretation of the references to colour in this figure legend, the reader is referred to the web version of this article.)



**Table 2**

Metrics comparison for resilient system operation (technical, economic, environmental and trade-off).

NO	Standard	Name	Mathematical Expression	Terms	Comment
(a)	Technical	Line Loading Percentage	$\frac{Current_{line}}{Rating_{max} \times df \times parallel}$	$Rating_{max}$ : maximum rating $df$ : derating factor $parallel$ : Number of parallel lines	Both maximum line loading rate and the system average loading rate are investigated (%)
(b)	Technical	Load Shedding Proportion	$\frac{SD-AC}{SD}$	$SD$ : System Demand $AC$ : Actual Consumption	The reduced load divided by the total system demand (%)
(c)	Economic	Short-Run Marginal Cost	$VOM + Fuel_{cost} \times Heat_{rate}$	$VOM$ : Operations & Maintenance Cost	The short-run marginal cost is computed in the DCOPF process (AU\$/MWh)
(d)	Environmental	Emission Factor	$\frac{\sum (Emission_{intensity} \times Gen)}{Total_{gen}}$	$Gen$ : Electricity Generation $Total_{gen}$ : Total Generation	System becomes eco-friendly as the emission factor decreases (kg CO <sub>2</sub> eq/kWh)
(e)	Comprehensive	Trade-off	Detailed explanation in Section 4		Load shedding cost VS DG cost

To be more specific, the coordinates in the Australian transmission line KML files are with a spatial resolution of 0.001° [44]. Thus, KML files were chosen here.

In terms of spatial information within the Wildfire Index, the original netCDF4 data of FWI were calculated for discontinuous grid cell vertices. To overlay the value over the entire region, each sampling point was first selected as the centre of one grid cell. Then the FWI of this grid region was assumed to have the average FWI of the four surrounding vertices.

#### 2.4. Combining wildfire and grid information

In combining the Wildfire Index with the Grid Model, methods to assess and determine the operational status of grid components are essential. As in most networks, transmission lines, especially high voltage lines, are geographically extended over a large area [45]; long transmission lines may cross different regions with separate and different wildfire risk conditions due to their microclimates. For instance, Victoria has a major transmission line (from Red Cliffs to Kerang), traversing different microclimates as shown and marked with green dots in Fig. 3. Long-extending transmission lines result in difficulties in making well-justified operational decisions as various line segments may have different failure probabilities.

Two main methods have been proposed to define the failure probability of system components that span multiple microclimate regions. The first utilised the weighted-average method: an incremental multiplier of failure rate (IMFR) can obtain the overall failure rate by adding the point-specific failure rates along each line segmentation according to their respective microclimate regions [46]. In the second category, the failure rate for the entire transmission line was determined by the highest failure rate along with any one single point of a line [47].

According to the Australian government, lines with a voltage greater than 66 kV are defined as transmission lines. Those at lower voltages are classified into the distribution level [48]. Thus, only transmission lines with voltage levels over 66 kV were considered in this paper. And the focus was given to cases in which transmission lines cross various microclimate regions. As shown in Fig. 3, most lines crossed different microclimates with different failure rates during the wildfire season. As minor failures can instantaneously have a great impact on the wider high-voltage transmission lines, this paper assumed that the worst failure rate along the line was selected to judge the whole line's failure and following operational modes.

The Test System operated according to simulated information from both the Wildfire Index and the Grid Model. The operation method here is similar to the real-world solution: transmission lines have reclosers installed which can be automatically disconnected if a fault or overload occurs [49]. To isolate the section of the power network under high fire risks and avoid a larger-scale outage, a controllable line-bus switch was set on each transmission line in the Test System [50]. While the worst line failure rate (depending on the worst fire risk exerting on the line) was available, the line operational mode was then controlled by line

switches. When any part of the transmission line crossed an area exceeding the preset risk threshold, the switch on the line was automatically disconnected. In Scenario 3, part of the network connected to a disconnected line would then operate in an islanded mode with DGs to reflect the operation of microgrids.

In the line disconnection decision process, the sampling accuracy can be changed according to the resolution of the data. For instance, since the grid cell length was 0.25° in Victoria, the coordinates along each line were extracted in steps of 0.01° latitude to achieve good spatial accuracy. After obtaining the transmission line coordinates, the corresponding FWI grid cell covering each line sampling point was identified. As the FWI of each regional cell had been computed, each coordinate along the line was assigned with a value of FWI.

Finally, the maximum FWI value was selected along each line and compared with the preset FWI threshold under different fire control conditions. A switch was opened within the Grid Model if the maximum FWI along a line exceeded the limit. Similarly, in practice, lines are disconnected to prevent wildfires, followed by customers being disconnected to ensure the power grid is not overloaded during wildfire seasons [51].

#### 2.5. Simulation methods

Grid performances (metrics from Table 2) were obtained from an optimal power flow model incorporating wildfire risk distributions [52]. The Optimal Power Flow (OPF) is the best operating situation of power stations to meet the grid demand, determined by network variables, constraints, and the specific objective of the OPF model utilised. The most common objective for OPF is to minimise operating costs [52]. OPF can be classified into Alternating Current OPF (ACOPF) and Direct Current OPF (DCOPF). ACOPF problems are typically approximated and solved by DCOPF that focuses exclusively on active power constraints due to its linearity and solvability [53].

The DCOPF is a built-in function in *pandapower*. The system completed the calculation procedures if the load and generation achieved balance with all constraints satisfied. According to the parameters of each generator, the optimal power flow followed the objective to minimise the system load shedding in the DCOPF. The Test System simulation was initialised using the wildfire, network, generator, historical load dispatch, and geospatial data. Then, DCOPF was carried out to produce system resilience parameters under different fire conditions.

Different metrics can be utilised as standards in grid resilience assessments, such as line loading percentage, load shedding percentage, increased economic profit, reduced death, ecological impact and so on [16]. The Short-Run Marginal Cost (SRMC) can describe the cost of producing one additional unit of service [54]. In the electricity market, SRMC is computed from the efficiency, operation and maintenance costs (O&M) and the fuel cost [55]. SRMC was utilised to evaluate the economic profit of the system in our study.

In the OPF result, four metrics were chosen for resilience analysis in

this paper. The performance parameters are displayed and explained in Table 2, which contains the technical, economic, and environmental standards as well as the measurement units.

### 3. Case study

In this section, the Test System prototype in Victoria, Australia, is first introduced, and then the details of three scenarios to analyse grid resilience performance are viewed. Of these, the first is to explore how overall wildfire risk levels affect grid resilience. Then two others are presented, i.e., preset FWI disconnection thresholds for lines and various capacities of dispatchable microgrids.

#### 3.1. The test system overview

To better apply the proposed methods to real-world network operations, a real power grid was selected in this paper. As mentioned in Section 1, Australia was attacked by a devastating wildfire from December 2019 to February 2020. Compared to other states in Australia, Victoria has some factors that make it suitable for a case study, such as large transmission networks, highly varying wildfire risks and good data availability. Thus, 'Victoria, Australia' (hereafter 'Victoria') in December 2019 has been selected as the research region of our case study.

Following the three steps explained in Section 2.2, the grid model for Victoria was built. In terms of the input for Step 1, 'Network Assembly', raw KML data from Geoscience Australia were utilised to obtain the electrical and geographical information on transmission lines [44], substations [56], and power stations [57]. State and boundary data in the format of shapefiles were accessed from the Australian Statistical Geography Standard in the Australian Bureau of Statistics [40]. According to the Regional Population Growth Module in the Australian Bureau of Statistics [41], the SA2 population datasets were obtained to estimate the regional demand distribution. NEM zones information were utilised to filter out operational grid components belonging to the Australian Energy Market Operator (AEMO) [43].

Then we moved to Step 2, 'Generator Dataset', the technical data of generators were collated from the Market Management System Data Model (MMSDM) [58]. The National Transmission Network Development Plan (NTNDP) database also contained information about the unit technical parameters and the operating costs [59]. The technical and economic generator dataset was constructed in Step 2.

As for Step 3, 'Historical Demand and Dispatch', the nodal demand proportion was obtained using the Voronoi tessellation method. The nodal demand was calculated by multiplying the nodal proportion by the total demand [58].

#### Main Components and Parameters

In this paper, the Victoria network was filtered so that only high voltage lines were retained. Thus, only lines with voltage levels over 66 kV were kept to focus on the high voltage system. Power stations with less than 5 MW ratings were also filtered as AEMO allowed standing exemptions for these small plants, which should not be categorised as generators [60]. There were 201 transmission lines within the NEM operational region in Victoria before the filter procedures. The information on the remaining system components is provided in the following paragraph (also displayed in Fig. 3).

There were 72 buses in the Test System with multiple voltage levels of 500 kV, 330 kV, and 220 kV. There were 68 transmission lines in the network, including  $16 \times 500$  kV lines,  $1 \times 330$  kV lines, and  $51 \times 220$  kV lines. 84 power stations were in operation in Victoria at the time of data collection, sourced by brown coal, natural gas, hydro, or wind.

#### The Test System Formulation and Simulation

A geographical rectangle region that could contain the entire Victoria territory was selected with the latitude range of  $[-39.25^\circ, -33.75^\circ]$  and the longitude range of  $[140.50^\circ, 150.00^\circ]$ . Since the resolution of FWI reanalysis data was  $0.25^\circ \times 0.25^\circ$ , the length and width of each grid

cell were both  $0.25^\circ$ . Thus, there were 836 grid cells in the selected research region in our model. It is noticeable that one degree represents different distances at different latitudes [61] (e.g.,  $0.25^\circ$  denote 28 km at  $0^\circ$ , whereas 22 km at  $36^\circ$ S in Victoria). As the latitude range of Victoria is not too wide, the side length of one grid cell can be regarded consistently as 22 km.

The initial system was simulated based on five days with varying wildfire risks to learn overall wildfire risk impacts on grid resilience in Scenario 1. The FWI line disconnection threshold and the DG proportion were varied in Scenarios 2 and 3 to explore how they may affect system resilience.

#### 3.2. Scenario overview

To start with, the original test system without microgrid integration was implemented based on the five-day data with different levels of wildfire risks. Different wildfire risk conditions can negatively impact line conductor temperatures and flowing current capacities [14]. Thus, the relationship between energy system resilience and the overall wildfire risk severity was studied in Scenario 1. The overall wildfire severity rose throughout December 2019. Therefore, five days were selected as these days can evenly represent the wildfire risk severity level growth from the lowest to the extreme in December ( $1^{\text{st}}$ ,  $3^{\text{rd}}$ ,  $5^{\text{th}}$ ,  $18^{\text{th}}$ ,  $30^{\text{th}}$ , December 2019). Fig. 4 displays various wildfire risk levels on the five selected days. The detail and the result analysis of each scenario will be discussed in Section 4.

The setting of FWI line disconnection thresholds may affect the system operation safety and effectiveness. To be more specific, each transmission line has a calculated FWI value, and more lines will be disconnected as the FWI disconnection threshold is set at a lower value. A lower FWI line disconnection threshold means achieving a stricter fire risk control circumstance. Scenario 2 aimed to explore how the FWI line disconnection threshold affected power grid resilience under different fire control conditions.

As the main objective of this paper, microgrid solutions were applied to mitigate the system burden during the wildfire season. As previously mentioned in Section 2.2, power demand at each node was obtained from the historical grid dispatch database [39]. A previous grid reinforcement project has proved that 75% of grid demand can be supported by microgrids, feasibly maintaining a normal operation [62]. In Scenario 3, the installation capacity of DGs was based on the node load in the Grid Model. Thus, 0%, 25%, 50% and 75% of the node load were selected as renewable capacities added at each node, respectively. The outage and microgrid costs were analysed and compared in this scenario.

## 4. Results and discussion

The results are analysed through technical, economic, and environmental aspects for each scenario. As mentioned in Table 2, four performance indices are obtained and assessed in each scenario, including system line loading percentage, load shedding rate, system operating cost and emission factor.

There were different operating cases defined for each scenario. In Scenario 1, five operating cases were selected from different days, representing different system fire risk levels. Three operating cases were set up in Scenario 2 with various FWI disconnection thresholds for power lines. In Scenario 3, four operating cases were defined based on various proportions of microgrid integration to the Test System.

#### 4.1. Scenario 1 overall wildfire level influences

In Scenario 1, the Test System was simulated with different levels of wildfire risks based on five-day data in December 2019. Both the average FWI and the maximum FWI in the Test System gradually rose from the operating case for  $1^{\text{st}}$  December to the operating case for  $30^{\text{th}}$

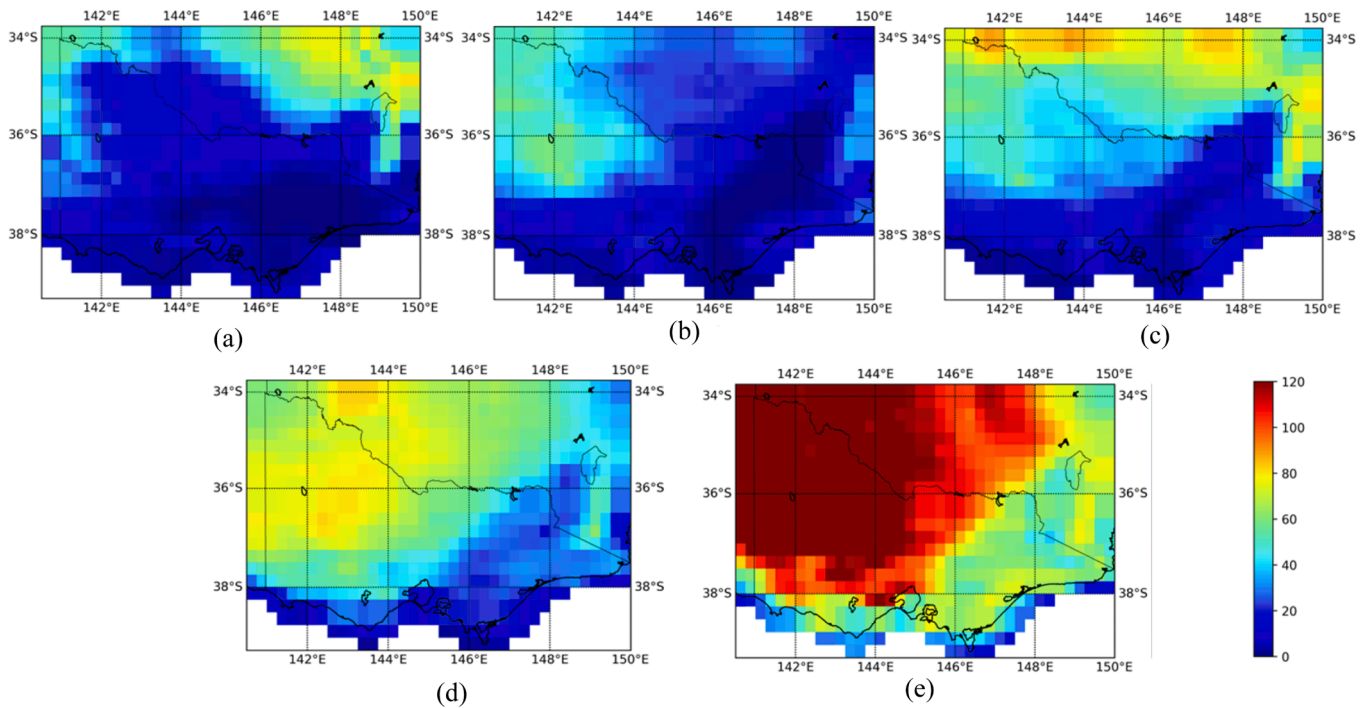


**Fig. 4.** Scenario 1: FWI colourmaps for five selected days in the 2019–2020 fire season in Victoria, Australia to explore the relationship between overall fire severity and grid resilience (1<sup>st</sup>, 3<sup>rd</sup>, 5<sup>th</sup>, 18<sup>th</sup>, 30<sup>th</sup> Dec 2019). An [animated video](#) displaying the dynamic FWI during the 2019–2020 Fire Season in Victoria, Australia, is linked here.

December. Since the demand may impact system resilience, grid demands of the following four operating cases were scaled down to the same for 1<sup>st</sup> December to control the variables (the total system demand).

Regions encounter an extreme wildfire risk if the FWI is greater than or equal to 50.0 [29]. In other words, the transmission line is likely to cause powerline ignition in this situation. Therefore, lines sitting in a grid cell with 50.0+ FWI were pre-disconnected automatically in Scenario 1.

Various lines were switched off as different numbers of lines exceeded the preset FWI threshold (50.0) in the five operating cases. The number of disconnected lines after the OPF simulation remained the same as before if there was no vast load shedding. However, compared to the initial number of pre-disconnected lines, due to a high FWI value, more lines were forced to become out of service if they violated the system safety conditions during the OPF simulation process. For instance, the initial FWI disconnection condition automatically switched off five lines in the operating case for 5<sup>th</sup> December. In contrast, the final disconnection rose to 22 out of 68 lines, as shown in Table 3, resulting in a large-scale blackout. Without the support of local DGs, large-scale outages can be more frequent due to higher wildfire risks.

As for the first evaluation metric, there was a slow growth in both the average and the maximum line loading percentages from 1<sup>st</sup> (85.88%,

131.76%), 3<sup>rd</sup> (86.27%, 149.23%) to 5<sup>th</sup> (86.63%, 163.64%). It is notable that the system loading sharply turned to drop in the last two days. The system loading was closer to zero in the next two operating cases as more lines were disconnected than pre-disconnected, causing a large-scale outage.

Moving to the second evaluation metric, the load shedding and the remaining load in Scenario 1 are displayed in Fig. 5. More lines were automatically switched off as the wildfire risk level increased, resulting in more load shedding. Nearly 100% of the load was curtailed in the operating case for 30<sup>th</sup> December.

The third evaluation is to assess the total and the unit system operational cost. As the wildfire risk developed, the total cost of operation gradually declined since the remaining operational grid was greatly curtailed due to a higher fire risk. Though the total amount decreased, the SRMC rose as the served demand dropped at a higher rate.

The Value of Lost Load (VoLL) represents the cost of disconnection to

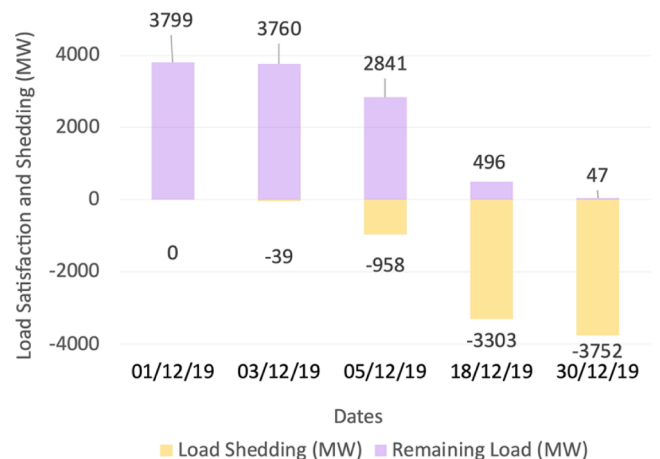


**Fig. 5.** Load shedding comparison for days with elevated fire conditions in Victoria, Australia (Scenario 1).

**Table 3**

Number of disconnected lines in Scenario 1. (Pre-OPF are lines switched off due to the exceeding of the preset high fire risk threshold before the OPF operation; post-OPF are regional power outages due to safety boundary violation after the OPF implementation).

Day	FWI Disconnected (Pre-OPF)	Actual Disabled (Post-OPF)
1 <sup>st</sup> Dec 2019	1	1
3 <sup>rd</sup> Dec 2019	2	2
5 <sup>th</sup> Dec 2019	5	22
18 <sup>th</sup> Dec 2019	17	62
30 <sup>th</sup> Dec 2019	68	68

customers [63]. It should be noted that VoLL was excluded from the simulated result of SRMC in all scenarios since VoLL can vary largely by season, time of the day, end-user demand and customer type (i.e., the VoLL for public infrastructures like hospitals is higher as the indirect loss for a power outage there is higher). VoLL was not necessarily used in the OPF simulation as the main objective of the OPF was to achieve minimum load shedding. However, the VoLL was still utilised in the cost-benefit analysis since it generally contributed to a significant cost increment [64].

With regarding to the fourth evaluation metric, in Scenario 1, there was no newly integrated renewable source, thus the generation fuel types determined the system's overall emission factor. The unit emission factor measured in kg CO<sub>2</sub>eq/kWh was mainly decided by the actual load consumption in this scenario. Overall emissions became lower from the start to the end of December due to the operational generation decreasing gradually under higher fire risks. As for the unit emission factor, the unit emission factor increased by 98.76% from 1<sup>st</sup> December to 30<sup>th</sup> December, as nearly all load was eventually shed. The grid became more polluting per kWh as the wildfire risk rose.

#### 4.2. Scenario 2 FWI line disconnection threshold

In Scenario 2, the Test System based on historical data from 1<sup>st</sup> December 2019 was tested with different FWI disconnection thresholds for power lines. According to the *Danger Rating* classification in Table 1, the FWI disconnection thresholds were set at extreme (50.0), very high (38.0), and high (21.3) in three operating cases, representing the fire control condition becoming stricter in Scenario 2.

Regarding the first evaluation metrics, both the maximum and the overall line loading percentages went up as the FWI disconnection threshold declined. Among the three operating cases, the average loading percentages retained the same order of magnitude (around 86%). In comparison, the maximum line loading gradually rose from 131.76% (operating case with the FWI threshold of 50.0) to 163.64% (operating case with the FWI threshold of 21.3) as more lines were disconnected due to a stricter limit of fire control.

For the second evaluation metric, as the FWI line threshold decreased, the load shedding increased as 7% of lines were pre-disabled in the third operating case, and the rest of the Grid Model could not hold the burden. The system maintained regular operation in the first two operating cases (with FWI thresholds of 50.0 & 38.0) since only one or two lines of 68 were switched off. However, the system load was sharply shed (25.21%) as five lines were pre-disconnected in the third operating case (with an FWI line disconnection threshold of 21.3).

The third evaluation metric is displayed in Fig. 6. The total and unit

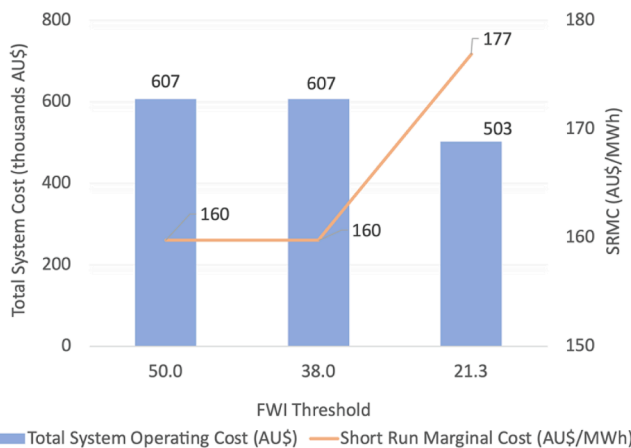


Fig. 6. System operating cost and SRMC with different fire control conditions. FWI thresholds set for transmission line disconnections at 50.0, 38.0, and 21.3, representing the fire control condition becoming stricter in Scenario 2.

operating costs in the first two operating cases (with the FWI thresholds of 50.0 and 38) remained the same since there was no load shedding in the first two operating cases, and the actual consumptions were the same. However, the total system operating cost dropped, and the unit operating cost rose once there was a load shedding, as shown in the third operating case. Thus, under a stricter fire risk control limit, the lower the FWI line disconnection threshold, the higher the unit cost.

Regarding the total system emissions, it remained at the same level as the threshold decreased. The unit carbon emission became higher as the actually served demand decreased from the loose fire control operating case (with the FWI threshold of 50.0) to the strict one (with the FWI threshold of 21.3).

Either an FWI of 38.0 or 50.0 can be selected as the disconnection threshold to prevent powerline wildfires which will not affect the normal operation of the Victoria system. The specific FWI threshold value will be judged by the actual needs in the wildfire control levels. If a greater requirement of wildfire control is expected, demand-side response (DSR) services should be integrated so that 100% of the load can be satisfied.

#### 4.3. Scenario 3 networked microgrids

In Scenario 3, dispatchable energy sources like DGs were integrated into the network with different capacity levels to mitigate load shedding. 0%, 25%, 50% and 75% of the node load capacity were injected with DGs at each node of the Grid Model in the four operating cases, respectively. In Scenario 3, the Test System based on historical data from 12<sup>th</sup> December 2019 was utilised since the Test System without microgrid support on this day had a load shedding of around 70% due to high wildfire risks. Various proportions of microgrid capacities were expected to alleviate the electrical outage to different extents. Cost-effectiveness was also evaluated and compared between load shedding compensation and microgrid connections budgets.

To begin with the first evaluation metric, Fig. 7 shows the maximum and the average line loading for four operating cases. As the DG capacity went up, the maximum and the overall system loading percentages decreased by 29.8% and 53.1%, respectively. The DG installation shared part of the local load, which led to a lower grid burden.

With the FWI threshold of 50.0 set in this scenario, 14 lines were switched off automatically to prevent large-scale outages due to fire control requirements before the OPF simulation process. Without microgrid supports, there would be substantial load shedding in the original network. In the first operating case without DGs, 36 more lines were indirectly disabled after the OPF simulation due to the 14 pre-disconnected lines. It was notable that no line was indirectly disconnected during OPF once DGs were installed to match 25% of the node

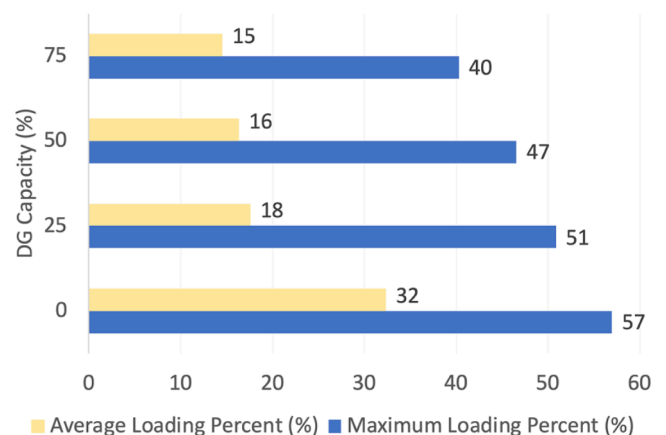


Fig. 7. Average and maximum system line loading percentages with various capacities of DG installation at each node in the grid (Scenario 3).



loads. As the DG integration level increased at the step of 25%, the load shedding gradually decreased (69.33%, 50.47%, 37.80%, 21.67%).

The Average Mitigating Rate (AMR) of load shedding between operating cases was obtained to assess how much load was recovered by DG integration. The method to calculate the rate is given in Eq. (1).

$$AMR = \frac{RL_{2nd} - RL_{1st}}{TSD} \times 100\% \quad (1)$$

where  $RL_{2nd}$  is the remaining load in the latter case (the 2<sup>nd</sup>, 3<sup>rd</sup>, and 4<sup>th</sup> operating cases),  $RL_{1st}$  is the remaining load in the former case (the 1<sup>st</sup>, 2<sup>nd</sup>, and 3<sup>rd</sup> operating cases),  $TSD$  is the total system demand.

The average mitigating rates between the four operating cases were 18.86%, 12.67% and 16.13%, respectively. The overall average mitigating rate was 15.89%, lower than the additional DGs (25%) between cases. Primarily because DGs only undertook the local demand at each node when the node was isolated. In addition, there were transmission power losses. Thus, the AMR was not just equal to 25% between every two operating cases.

Regarding to the economic evaluation in Fig. 8, the total system operating cost in the first column was relatively lower since 70% of the load was shed in the first operating case without microgrids. In the subsequent three operating cases, there was a surge of 9% in the total system cost first. Then it gradually decreased as cheaper DGs were connected (the O&M cost comparison of DGs and fossil fuel plants will be discussed in Section 4.4). The increase in the total system cost was caused by the system recovery after DG integrations.

The average system operating cost decreased as more local generations came onto the network. For one reason, the overall system operating cost decreased since the SRMC of renewables was much lower than the centralised fossil generation. In addition, the scale of actual consumption recovered as the DG developed. As displayed in Fig. 9, the total and unit emissions decreased as more renewable DGs were used, and the actual consumption rose. Both the unit operating cost and the unit carbon emission decreased as more DGs were used.

#### 4.4. Cost-benefit analysis for microgrid solutions

There are various natural resources for renewable energy in Victoria, including wind, hydro, solar, and bioenergy. The existing widely distributed onshore wind farms and ongoing offshore wind farm projects have proved the feasibility of wind power utilisation in Victoria [65]. Victoria is an excellent site for wind power generation with an average wind speed measured at  $6.5 \text{ ms}^{-1}$  [66].

In this paper, we propose hypothetical planning of renewable utilisation in Victoria. Both wind and solar resources are abundant in Victoria. A demonstration of renewable resource distribution in Victoria is shown in Fig. 10. Referring to the Victorian transmission network in

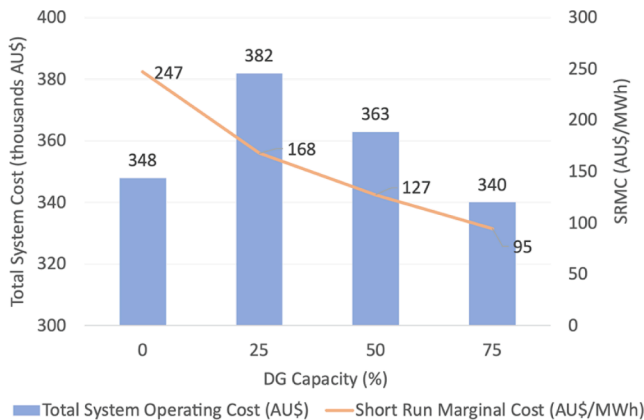


Fig. 8. System cost and SRMC with various capacities of DG installation at each node in the grid (Scenario 3).

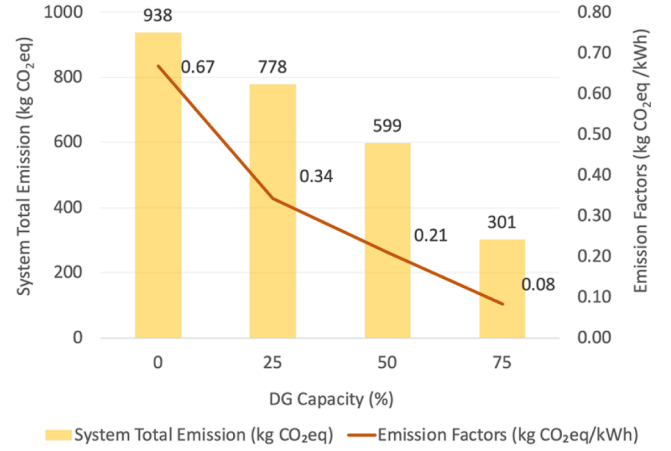


Fig. 9. System emission factors with various capacities of DG installation at each node in the grid (Scenario 3).

Fig. 3 and the FWI maps in Fig. 4, wind resource distribution is highly colocated with both the fire risk and the network distribution than solar power. Furthermore, there is a positive correlation between wind speed and wildfire spread [67], i.e., fire-prone areas are likely to have greater wind power potential. There is a relatively high coincident distribution between the wind abundance and the severe fire risk. In addition, wind power operates more reliably diurnally than solar power. As mentioned in Section 1, wildfire smoke can negatively affect solar generation efficiency. Therefore, we would select wind as the DG source as an example here [68,69].

The microgrid strategies can enhance system resilience by reducing load shedding during the period of high wildfire risks. Then, the financial losses brought by the load shedding can be eased by microgrid installations. However, the installation of the local DGs requires both the capital investment and the O&M cost. The trade-off between the saved cost for load shedding and the lifetime budget for DG installation is assessed in this section.

The system costs before and after the DG installation were compared based on Eq. (2).

$$SO_{cost} = TS_{cost} + VoLL + DG_{cost} \quad (2)$$

where  $SO_{cost}$  is the Test System overall cost,  $TS_{cost}$  is the total system cost which can be obtained from the OPF;  $VoLL$  contains the economic impact of load shedding (through multiplying the unit  $VoLL$  cost by the load shedding); Levelised Cost of Electricity (LCOE) assesses the cost of generation for a generator over its lifespan, considering the capital cost and the O&M cost together [70];  $DG_{cost}$  is calculated by multiplying the DG capacity by the LCOE of a wind turbine in Victoria.

According to the Australian Energy Regulator [71], the average electricity price for the Victoria network was AU\$84/MWh in 2019. Referring to the latest 2021 economic analysis report about power grids in the NEM, the NEM's Market Price Cap of AU\$15,000/MWh is almost the highest in the world [72]. Thus, we assume the  $VoLL$  induced by outages in the scenario without DGs amounted to AU\$15,000/MWh as an upper limit here. According to statistics from IRENA (International Renewable Energy Agency) [73], the LCOE of a wind turbine was assumed to be AU\$64/MWh. The capacity factor of wind turbines was assumed to be 41% [74], which should be considered in the real cost of DGs, as expressed in Eq. (3).

$$DG_{cost} = (DG_{gen} \div CF) \times LCOE \quad (3)$$

where  $DG_{cost}$  is the project cost for DG installation,  $DG_{gen}$  is the DG generation,  $CF$  is the capacity factor.

The data from Scenario 3 were analysed in Table 4, with various proportions of DG connections (the total system demand was 4,587

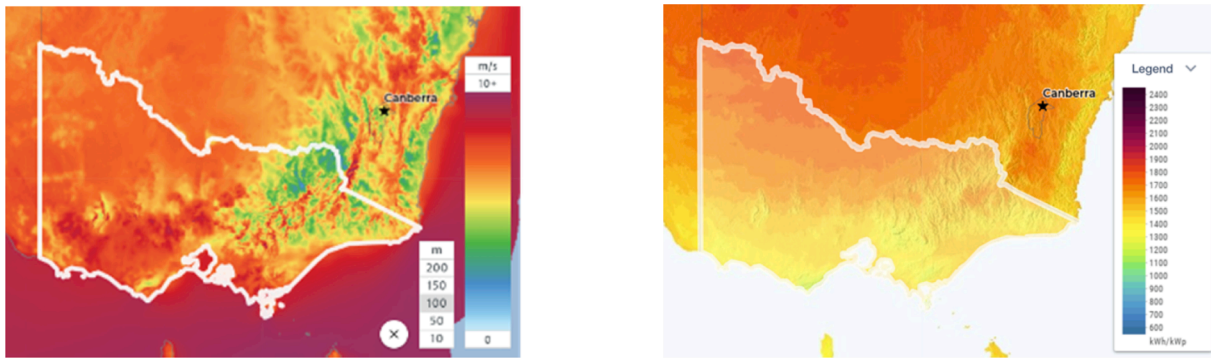


Fig. 10. Distribution maps of renewable resources in Victoria, Australia. Left: mean wind speed ( $\text{ms}^{-1}$ ) [68]. Right: mean PV power output ( $\text{kWh/kWp}$ ) [69].

Table 4

Cost analysis between intentioned outages without DGs and different proportions of DG installation plans in Scenario 3.

DG Penetration (%)	DG Capacity (MW)	DG Cost (AU\$)	Load Shedding (MW)	VoLL (AU\$)	Operating Cost (AU\$)	Overall Cost (AU\$)
0	0	0	3,180	47,700,000	348,000	48,048,000
25	1,147	179,000	2,315	34,725,000	382,000	35,107,000
50	2,294	358,000	1,734	26,010,000	363,000	26,373,000
75	3,440	537,000	994	14,910,000	340,000	15,250,000

MW). The calculation was based on Eq. (2). The  $DG_{\text{cost}}$  went up as more wind turbines were connected to the system. VoLL represented the economic impact caused by load shedding, which was mitigated as more DGs were integrated. The total system operating cost was obtained directly from the OPF simulation, reflecting the system operating cost in various circumstances. The overall cost considering all above was summed up in the last column. The total economic impact was alleviated as more DGs were installed in the Test System. Compared to the initial system, around 68% of the overall cost was eased when the local DGs supplemented 75% of nodal demand. The considerably high VoLL in NEM took the dominant role here as a leading factor in overall system cost saving. Thus, the local renewable generation method was considered a financially viable solution to achieve a more resilient power network in Victoria, Australia.

#### 4.5. System summary

Among the three scenarios, factors that affect system resilience, economy and environment were simulated and investigated, i.e., the overall fire risk level, the FWI line disconnection threshold and different proportions of microgrid installations.

With regard to power system load shedding, DG produced generation mitigated the curtailed demand in a financially feasible way. The unit operational cost was mainly affected by the consumed system demand and the total system cost. The higher the DG proportion, the lower the unit cost. The unit carbon emission factor mainly depended on the served energy consumption, calculated from the OPF simulation. The summary of effects is given in Table 5. (where '+' represents an

increasing variable and '-' represents a declining variable)

#### 5. Conclusion and future work

This paper has proposed the use of microgrids as a novel strategy to mitigate powerline fire risks without the need for blackouts. The power system resilience performance was assessed in high wildfire risk regions. Victoria, Australia, in December 2019 was selected as an example case study. This paper was driven by the practical need to protect power systems and reduce economic and social loss during a high wildfire risk period. The results obtained from the simulations have shown how can intentional power shut offs and microgrids enhance power system resilience in a financially feasible way. The validated FWI was first utilised in a weather-affected power system, which improved the spatial and temporal resolution of wildfire risk positioning in power grids.

Methodologies to assess grid resilience and to build the weather-affected energy system were introduced and discussed. The controllable power line switch played the role of the bridge between the Wildfire Index and the Grid Model, which was automatically disconnected as the line FWI exceeded the preset thresholds under different fire control conditions. The methodology does not exclusively apply to the Test System in Victoria but can be adjusted to other fire-prone regions, supporting the use of the applied methods across various spatial domains and wildfire-prone network grids.

Three scenarios were presented to investigate how the Test System was influenced by three main variables, i.e., the overall wildfire risk level, the FWI disconnection thresholds for power lines, and the microgrid proportions.

The results showed that the overall line loading percentage was positively correlated with the wildfire risk. The line loading percentage declined as the FWI threshold or the DG proportion went up. Secondly, the change of load shedding had an opposite tendency with the FWI threshold and DG capacity, and load shedding rose as the wildfire risk became higher. As for the unit operational costs, only the severity of wildfire risk negatively impacted costs. The unit carbon emission factor was eased as the FWI thresholds or the DGs increased, but it was worse as the wildfire risk became more severe.

A higher value in the FWI disconnection thresholds and DG capacities eased system operational stress, both economically and

Table 5

The Test System performance comparison (where '+' stands for an increasing trend and '-' represents a declining trend).

Performances	Scenarios		
	I	II	III
Variable Tendency (+)	Fire Risk	FWI Threshold	DGs
Line Loading Percentage	+	—	—
Load Shedding	+	—	—
Unit Operational Cost	+	—	—
Unit Emission Factor	+	—	—

environmentally. According to the cost-benefit analysis, it was proved that the microgrid solution could save 68% of the overall system cost. It provided both a way to improve system resilience economically and feasibly integrate more renewables within the grid.

FWI data are currently measured daily, at noon Local Standard Time worldwide. However, power systems are usually assessed once every half hour. A more accurate model can be obtained as the temporal resolution of the weather data becomes higher. An FWI curve with a temporal resolution at half-hour intervals can be linearly formed by FWI related parameter curves.

Since the *pandapower* is not directly a time-dependent tool for power simulations, no time domain parameter is set in the default power flow calculations. The current system can only model instantaneous and static operations. More frequent monitoring of the grid operation is therefore preferred. More scenarios can be designed in a continuous-time model when energy flow is created rather than just instantaneous power flow, e.g., scenarios about energy storages.

While our paper only assesses the transmission network with voltage levels greater than 66 kV, the model can be applied to a lower voltage level network to explore electrically caused wildfires and wildfire-induced electrical faults in distribution networks in the future.

In conclusion, the high-resolution wildfire-affected power grid combining the FWI, intelligent power line disconnection strategies, and microgrid solutions was proposed in this paper. It has been demonstrated that microgrids have the potential to improve grid resilience performances economically. The methods developed for weather-dependent power system modelling in this paper can be used to investigate how microgrids improve power grid resilience in the face of other extreme weather events, such as floods and hurricanes in the future.

#### CRedit authorship contribution statement

**Weijia Yang:** Methodology, Software, Writing – original draft, Writing – review & editing. **Sarah Sparrow:** Writing – review & editing, Methodology, Supervision. **Masao Ashtine:** Writing – review & editing, Supervision. **David Wallom:** Conceptualization, Writing – review & editing, Supervision. **Thomas Morstyn:** Conceptualization, Methodology, Writing – review & editing, Supervision.

#### Declaration of Competing Interest

The authors declare that they have no known competing financial interests or personal relationships that could have appeared to influence the work reported in this paper.

#### Acknowledgement

The author would like to acknowledge that this work is supported by the UK Centre for Greening Finance and Investment (CERAF) (NERC grant NE/V017756/1); the Newton Fund through the Met Office Weather and Climate Science for Service Partnership Brazil (WCSSP Brazil) (NF\_MO\_BRA\_491); the Local Energy Oxfordshire project (IUK #104781), and the UK Engineering and Physical Sciences Research Council (EPSRC) funded EnergyReV project (EP/S031901/1).

#### Appendix A. Supplementary material

Supplementary data to this article can be found online at <https://doi.org/10.1016/j.apenergy.2022.118793>.

#### References

- [1] Frame DJ, Rosier SM, Noy I, Harrington LJ, Carey-Smith T, Sparrow SN, et al. Climate change attribution and the economic costs of extreme weather events: a study on damages from extreme rainfall and drought. *Climatic Change* 2020;162(2):781–97. <https://doi.org/10.1007/s10584-020-02729-y>.

- [2] Clarke H, Gibson R, Cirulis B, Bradstock RA, Penman TD. Developing and testing models of the drivers of anthropogenic and lightning-caused wildfire ignitions in south-eastern Australia. *Journal of Environmental Management* 2019;235:34–41. <https://doi.org/10.1016/j.jenvman.2019.01.055>.
- [3] Syphard AD, Keeley JE. Location, timing and extent of wildfire vary by cause of ignition. *International Journal of Wildland Fire* 2015;24:37–47. <https://doi.org/10.1071/WF14024>.
- [4] Rhodes N, Ntamo L, Roald L. Balancing wildfire risk and power outages through optimized power shut-offs. *IEEE Transactions on Power Systems* 2021;36(4):3118–28. <https://doi.org/10.1109/TPWRS.2020.3046796>.
- [5] Sathaye J, Dale L, Larsen P, Fitts G, Koy K, Lewis S, et al. Estimating risk to California energy infrastructure from projected climate change, 2011.
- [6] Fire and high voltage transmission line safety – information sheet. *POWERLINK Queensland* 2015.
- [7] Filkov AI, Ngo T, Matthews S, Telfer S, Penman TD. Impact of Australia's catastrophic 2019/20 bushfire season on communities and environment. Retrospective analysis and current trends. *Journal of Safety Science and Resilience* 2020;1(1):44–56. <https://doi.org/10.1016/j.jnlssr.2020.06.009>.
- [8] State Library Victoria. 2019–20 Bushfires in Victoria – Research Guides. State Library Victoria 2020. <https://guides.slv.vic.gov.au/bushfires/2019>.
- [9] The 2019–20 bushfires: a CSIRO explainer. CSIRO 2020. <https://www.csiro.au/en/research/natural-disasters/bushfires/2019-20-bushfires-explainer>.
- [10] Endeavour Energy. Cost pass through application 2019–20 Bushfire disaster event; 2020. <https://www.aer.gov.au/system/files/Endeavour%20Energy%20-%202019-20%20bushfire%20disaster%20event%20cost%20pass%20through%20-%20Application%20-%20August%202020.pdf> [accessed April 22, 2021].
- [11] Penn I, Eavis P. PG&E pleads guilty to 84 counts of manslaughter in camp fire case. *The New York Times*; 2020.
- [12] EIA. Delivery to consumers – U.S. Energy Information Administration (EIA), 2020. <https://www.eia.gov/energyexplained/electricity/delivery-to-consumers.php>.
- [13] Baker DR. Underground power lines don't cause wildfires. But they're really expensive. *San Francisco Chronicle*; 2017. <https://www.sfchronicle.com/bayarea/article/Underground-power-lines-don-t-cause-wildfires-12295031.php>.
- [14] Trakas DN, Hatziaargyriou ND. Optimal distribution system operation for enhancing resilience against wildfires. *IEEE Transactions on Power Systems* 2018;33(2):2260–71.
- [15] Bie Z, Lin Y, Li G, Li F. Battling the extreme: a study on the power system resilience. *Proceedings of the IEEE* 2017;105(7):1253–66.
- [16] Willis HH, Loa K. Measuring the resilience of energy distribution systems. *RAND Corporation* 2015.
- [17] Dyson M, Li B. Reimagining grid resilience a framework for addressing catastrophic threats to the US electricity grid in an era of transformational change, 2020.
- [18] Guo Y, Zhao C. Islanding-aware robust energy management for microgrids. *IEEE Transactions on Smart Grid* 2018;9(2):1301–9.
- [19] Funabashi T. Integration of distributed energy resources in power systems: implementation, operation and control. Elsevier Inc; 2016. <https://doi.org/10.1016/C2014-0-03911-1>.
- [20] Jazebi S, de Leon F, Nelson A. Review of wildfire management techniques-Part I: Causes, prevention, detection, suppression, and data analytics. *IEEE Transactions on Power Delivery* 2020;35(1):430–9. <https://doi.org/10.1109/TPWRD.2019.2930055>.
- [21] Jazebi S, de Leon F, Nelson A. Review of wildfire management techniques-Part II: Urgent call for investment in research and development of preventative solutions. *IEEE Transactions on Power Delivery* 2020;35(1):440–50. <https://doi.org/10.1109/TPWRD.2019.2930095>.
- [22] Perry M, Troccoli A. Impact of a fire burn on solar irradiance and PV power. *Solar Energy* 2015;114:167–73. <https://doi.org/10.1016/J.SOLENER.2015.01.005>.
- [23] Stephen York. Smoke from California wildfires decreases solar generation in CAISO – Today in Energy – U.S. Energy Information Administration (EIA). EIA 2020. <https://www.eia.gov/todayinenergy/detail.php?id=45336>.
- [24] Ya'acobi M. E., Hizam H., Adam M. B., Rahim A. H. M. A., Radzi M. A. M., Hashimoto Y., et al. Decreasing of grid-tied PV power output due to thick haze phenomena in Malaysia. In: 2014 Saudi Arabia smart grid conference, SASG 2014. <https://doi.org/10.1109/SASG.2014.7274288>.
- [25] Hoseinzadeh B., Amini M. H., Bak C. L. Centralized load shedding based on thermal limit of transmission lines against cascading events, 2016.
- [26] Duginski P. Strong winds and high fire danger expected in Northern California this weekend. *Los Angeles Times*; 2019.
- [27] National Wildfire Coordinating Group. Fire Weather Index (FWI) System. NWCG 2021. <https://www.nwcg.gov/publications/pms437/cffdrs/fire-weather-index-system>.
- [28] Copernicus. Fire danger indices historical data from the Copernicus Emergency Management Service. Copernicus 2019. <https://cds.climate.copernicus.eu/cdsapp#!/dataset/cems-fire-historical?tab=form>.
- [29] Copernicus. Fire index user guide. Copernicus; 2017. [http://datastore.copernicus-climate.eu/c3s/published-forms/c3sprod/cems-fire-historical/Fire\\_In\\_CDS.pdf](http://datastore.copernicus-climate.eu/c3s/published-forms/c3sprod/cems-fire-historical/Fire_In_CDS.pdf).
- [30] Dowdy AJ, Mills GA, Finkele K, Groot W. Australian fire weather as represented by the McArthur Forest Fire Danger Index and the Canadian Forest Fire Weather Index. *Bureau of Meteorology, Australian Government*; 2009.
- [31] Dowdy AJ, Mills GA, Finkele K, de Groot W. Index sensitivity analysis applied to the Canadian Forest Fire Weather Index and the McArthur Forest Fire Danger Index. *Meteorological Applications* 2010;17(3):298–312. <https://doi.org/10.1002/met.170>.



- [32] van Oldenborgh G, Krieken F, Lewis S, Leach NJ, Lehner F, Saunders KR, et al. Attribution of the Australian bushfire risk to anthropogenic climate change. *Natural Hazards and Earth System Sciences* 2020. <https://doi.org/10.5194/nhess-2020-69>.
- [33] Camia A, Amatulli G. Weather factors and fire danger in the mediterranean. *Earth Observation of Wildland Fires in Mediterranean Ecosystems*. In: Chuvieco E, editor. Springer Berlin Heidelberg; 2009. p. 71–82.
- [34] Dimitrakopoulos AP, Benmerzouk AM, Mitsopoulos ID. Evaluation of the Canadian fire weather index system in an eastern Mediterranean environment. *Meteorological Applications* 2011;18(1):83–93. <https://doi.org/10.1002/met.214>.
- [35] netCDF4 API documentation. NetCDF4 API; 2019. <https://unidata.github.io/netcdf4-python/> [accessed April 20, 2021].
- [36] Luo Y, Zhou X. Temporal and spatial variations in soil respiration. *Soil Respiration and the Environment* 2006;107–31. <https://doi.org/10.1016/B978-012088782-8/50006-1>.
- [37] França GB, Oliveira AN, Paiva CM, Peres L, Oliveira LMT. A fire-risk-breakdown system for electrical power lines in the North of Brazil. *Journal of Applied Meteorology and Climatology* 2013. <https://www.jstor.org/stable/26176341?reqid=excelsior%3A4d44ca2b89e1b745051f267c1ac26cd7>.
- [38] Google Developers. Keyhole markup language. Google developers 2021. <http://developers.google.com/kml>.
- [39] Xenophon A, Hill D. Open grid model of Australia's national electricity market allowing backtesting against historic data. *Scientific Data* 2018;5:1–21. <https://doi.org/10.1038/sdata.2018.203>.
- [40] Australian Bureau of Statistics. Australian Statistical Geography Standard. Australian Bureau of Statistics; 2016. <https://www.abs.gov.au/AUSSTATS/abs@.nsf/DetailsPage/1270.0.55.003July%202016?OpenDocument>.
- [41] Australian Bureau of Statistics. Regional population growth, Australia. Australian Bureau of Statistics; 2016. <https://www.abs.gov.au/AUSSTATS/abs@.nsf/DetailsPage/3218.02014-15?OpenDocument>.
- [42] Ju L, Ringer T, Gunzburger M. Voronoi tessellations and their application to climate and global modelling. U.S. Department of Energy Office of Scientific and Technical Information; 2012. <https://www.osti.gov/servlets/purl/1090872>.
- [43] AEMO. The national electricity market FACT SHEET 2020. <https://aemo.com.au/-/media/files/electricity/nem/national-electricity-market-fact-sheet.pdf>.
- [44] Geoscience Australia. Geoscience Australia – electricity transmission lines. Geoscience Australia 2019. <https://ecat.ga.gov.au/geonetwork/srv/eng/catalog.search#/metadata/83105>.
- [45] Arderne C, Zorn C, Nicolas C, Koks EE. Predictive mapping of the global power system using open data. *Scientific Data* 2020;7:1–12. <https://doi.org/10.1038/s41597-019-0347-4>.
- [46] Liu Y, Singh C. A methodology for evaluation of hurricane impact on composite power system reliability. *IEEE Transactions on Power Systems* 2011;26(1):145–52. <https://doi.org/10.1109/TPWRS.2010.2050219>.
- [47] Panteli M, Mancarella P. Influence of extreme weather and climate change on the resilience of power systems: Impacts and possible mitigation strategies. *Electric Power Systems Research* 2015;127:259–70. <https://doi.org/10.1016/j.epsr.2015.06.012>.
- [48] Government of South Australia. Identifying powerlines. Government of South Australia 2017. <https://www.sa.gov.au/topics/energy-and-environment/using-electricity-and-gas-safely/powerline-safety/identifying-powerlines>.
- [49] Eaton. Recloser technical data; 2017. [www.eaton.com/cooperpowerseries](http://www.eaton.com/cooperpowerseries).
- [50] Thurner L, Scheidler A, Schafer F, Menke J-H, Dollichon J, Meier F, et al. Pandapower – an open-source python tool for convenient modeling, analysis, and optimization of electric power systems. *IEEE Transactions on Power Systems* 2018; 33(6):6510–21. <https://doi.org/10.1109/TPWRS.2018.2829021>.
- [51] National Grid. Guidance for UK fire and rescue services. National Grid 2018. [https://www.nationalgrid.com/sites/default/files/documents/FINAL\\_Fire%20%26%20Rescue.pdf](https://www.nationalgrid.com/sites/default/files/documents/FINAL_Fire%20%26%20Rescue.pdf).
- [52] Sheble GB, McCalley JD. Module E3 economic dispatch calculation. Iowa State University; 2019.
- [53] Sun J, Tesfatsion L, Goldfarb D, Hogan W, Kirschen D, Liu C-C, et al. DC optimal power flow formulation and solution using QuadProgJ\*. Iowa State University 2010.
- [54] John A. Dutton e-Education Institute. Variable cost concepts for power generation. Pennsylvania State University 2019. <https://www.e-education.psu.edu/ebf483/node/584>.
- [55] Moye R, Meyn S. The use of marginal energy costs in the design of U.S. Capacity Markets; 2018. <https://core.ac.uk/download/pdf/143481163.pdf> [accessed May 5, 2021].
- [56] Geoscience Australia. Geoscience Australia – Electricity Transmission Substations. Geoscience Australia; 2019. <https://ecat.ga.gov.au/geonetwork/srv/eng/catalog.search#/metadata/83173>.
- [57] Geoscience Australia. Geoscience Australia – power stations. Geoscience Australia 2019. <https://ecat.ga.gov.au/geonetwork/srv/eng/catalog.search#/metadata/82326>.
- [58] AEMO. AEMO Market data. NEMWEB 2020. <https://www.aemo.com.au/energy-systems/electricity/national-electricity-market-nem/data-nem/market-data-nemweb#mms-data-model>.
- [59] AEMO. NTNDP database; 2020. <https://www.aemo.com.au/energy-systems/major-publications/integrated-system-plan-isp/national-transmission-network-k-development-plan-ntndp/ntndp-database> [accessed April 28, 2021].
- [60] AEMO. Guide to generator exemptions and classification of generating units; 2021. [https://www.aemo.com.au/-/media/Files/Electricity/NEM/Participant Information/New-Participants/Generator-Exemption-and-Classification-Guide.docx](https://www.aemo.com.au/-/media/Files/Electricity/NEM/Participant%20Information/New-Participants/Generator-Exemption-and-Classification-Guide.docx) [accessed April 28, 2021].
- [61] USGS. How much distance does a degree, minute, and second cover on your maps? 2018. [https://www.usgs.gov/faqs/how-much-distance-does-a-degree-minute-and-second-cover-your-maps?qt-news\\_science\\_products=0#qt-news\\_science\\_products](https://www.usgs.gov/faqs/how-much-distance-does-a-degree-minute-and-second-cover-your-maps?qt-news_science_products=0#qt-news_science_products) [accessed June 10, 2021].
- [62] Energy Exemplar. Understanding microgrids; their impact and integration in a complex energy environment; 2020. [https://energyexemplar.com/wp-content/uploads/EE\\_eBook\\_Microgrids.pdf](https://energyexemplar.com/wp-content/uploads/EE_eBook_Microgrids.pdf) [accessed May 5, 2021].
- [63] OFGEM DECC. The value of lost load (VoLL) for electricity in Great Britain. OFGEM 2013. <https://www.ofgem.gov.uk/ofgem-publications/82293/london-economic-s-value-lost-load-electricity-gbp.pdf>.
- [64] Schröder T, Kuckshinrichs W. Value of lost load: An efficient economic indicator for power supply security? A literature review. *Frontiers in Energy Research* 2015; 3. <https://doi.org/10.3389/fenrg.2015.00055>.
- [65] Victoria State Government. Renewable energy action plan 2017 Statement of Progress. Victoria State Government 2017. [https://www.energy.vic.gov.au/\\_data/assets/pdf\\_file/0014/113432/DELWP006-REAP-SOP\\_F.pdf](https://www.energy.vic.gov.au/_data/assets/pdf_file/0014/113432/DELWP006-REAP-SOP_F.pdf).
- [66] Geoscience Australia. Wind Energy | Geoscience Australia, 2010. <https://www.ga.gov.au/scientific-topics/energy/resources/other-renewable-energy-resources/wind-energy>.
- [67] Muhs JW, Parvania M, Nguyen HT, Palmer JA. Characterizing probability of wildfire ignition caused by power distribution lines. *IEEE Transactions on Power Delivery* 2021;36(6):3681–8. <https://doi.org/10.1109/TPWRD.2020.3047101>.
- [68] Global Wind Atlas. Energy data info, 2021 <https://globalwindatlas.info/>.
- [69] Global Solar Atlas. Energy data info, 2021. <https://globalsolaratlas.info/map?c=-35.201256,144.148881,6&r=AUS.10.1>.
- [70] Energy Information Administration U. Levelized Costs of New Generation Resources in the Annual Energy Outlook 2021; 2021. [https://www.eia.gov/outlooks/aeo/pdf/electricity\\_generation.pdf](https://www.eia.gov/outlooks/aeo/pdf/electricity_generation.pdf) [accessed May 5, 2021].
- [71] Wholesale statistics. Australian energy regulator 2021. <https://www.aer.gov.au/wholesale-markets/wholesale-statistics>.
- [72] Simshauser P. Rooftop solar PV and the peak load problem in the NEM's Queensland region; 2021.
- [73] Renewable power generation costs in 2018. IRENA 2018. [https://www.irena.org/-/media/Files/IRENA/Agency/Publication/2019/May/IRENA\\_Renewable-Power-Generations-Costs-in-2018.pdf](https://www.irena.org/-/media/Files/IRENA/Agency/Publication/2019/May/IRENA_Renewable-Power-Generations-Costs-in-2018.pdf).
- [74] Blakers A, Lu B, Stocks M. 100% renewable electricity in Australia. *Energy* 2017; 133:471–82. <https://doi.org/10.1016/j.energy.2017.05.168>.